Evidence for Deleterious Original Antigenic Sin in SARS-CoV-2 Immune Response

Sanjana R. Sen[1], Emily C. Sanders[2], Alicia M. Santos[2], Keertna Bhuvan[2], Derek Y. Tang[2], Aidan A. Gelston[2], Brian M. Miller[2], Joni L. Ricks-Oddie[3,4] and Gregory A. Weiss[1,2,5]*

Author Affiliations:

[1] Department of Molecular Biology & Biochemistry, University of California, Irvine, Irvine CA 92697-3900 USA
[2] Department of Chemistry, University of California, Irvine, Irvine CA 92697-2025 USA
[3] Center for Statistical Consulting, Department of Statistics, University of California, Irvine, Irvine CA 92697-1250 USA
[4] Biostatics, Epidemiology and Research Design Unit, Institute for Clinical and Translational Sciences, University of California, Irvine, Irvine CA 92697-4094 USA
[5] Department of Pharmaceutical Sciences, University of California, Irvine, Irvine CA 92697-3958 USA

* Address correspondence to gweiss@uci.edu

Corresponding Author:

*GAW e-mail: gweiss@uci.edu, Tel: +1-949-824-5566, address: 1102 Natural Sciences 2, Irvine, CA 92697-2025, USA

Author Contributions:

S.R.S., and G.A.W. designed research; S.R.S., E.C.S., A.M.S., K.B., D.Y.T, A.A.G., and B.M.M. performed research; S.R.S., E.C.S. and G.A.W. analyzed data; J.L.R. advised on statistical analysis; S.R.S. and G.A.W. wrote the manuscript.

Competing Interests:

None.

Acknowledgements:

We thank Professor Elizabeth Bess and Professor Stacey Schultz-Cherry for helpful conversations, Kristin Gabriel for initial bioinformatics analysis, and the patients who generously donated their plasma samples (IRB# 2012-8716). We gratefully acknowledge the support of the UCI COVID-19 Basic, Translational and Clinical Research Fund (CRAFT), the Allergan Foundation, and UCOP Emergency COVID-19 Research Seed Funding. G.S.S and A.M.S thank the Minority Access to Research Careers (MARC) Program, funded by the NIH (GM-69337). J.L.R. was supported by the National Center for Research Resources and the National Center for Advancing Translational Sciences from the NIH (TR001414).

Abstract

A previous report demonstrated the strong association between the presence of antibodies binding to an epitope region from SARS-CoV-2 nucleocapsid, termed Ep9, and COVID-19 disease severity. Patients with anti-Ep9 antibodies (Abs) had hallmarks of original antigenic sin (OAS), including early IgG upregulation and cytokine-associated injury. Thus, the immunological memory of a previous infection was hypothesized to drive formation of suboptimal anti-Ep9 Abs in severe COVID-19 infections. This study identifies a putative original antigen capable of stimulating production of cross-reactive, anti-Ep9 Abs. From bioinformatics analysis, 21 potential “original” epitope regions were identified. Binding assays with patient blood samples directly show cross-reactivity between Abs binding to Ep9 and only one homologous potential antigen, a sequence derived from the neuraminidase protein of H3N2 Influenza A virus. This cross-reactive binding affinity is highly virus strain specific and sensitive to even single amino acid changes in epitope sequence. The neuraminidase protein is not present in the influenza vaccine, and the anti-Ep9 Abs likely resulted from the widespread influenza infection in 2014. Therefore, OAS from a previous infection could underlie some cases of COVID-19 disease severity and explain the diversity observed in disease outcomes.

Introduction

Original antigenic sin (OAS) occurs when the immune responses adapted for a primary (or "original") infection instead target a similar, but not identical, pathogen (Fierz & Walz, 2020). Since B-cells undergo affinity maturation post-primary infection, affinity-matured Abs from previous infections can sometimes outcompete naïve Abs with specificity for the new antigen (Brown & Essigmann, 2021). The phenomenon has been observed for immune responses to dengue fever, influenza, respiratory syncytial virus and human immunodeficiency virus (HIV) (Park, Kim, Park, Lee, & Park, 2016; Welsh & Fujinami, 2007). OAS ideally accelerates pathogen clearance by targeting highly conserved antigens; however, suboptimal targeting by non-neutralizing Abs binding to the antigen can exacerbate disease conditions by either enhancing viral infection or hyperactivating the innate immune response (Brown & Essigmann, 2021). The wide range of outcomes observed in SARS-CoV-2 infected individuals, from asymptomatic to fatal, has been hypothesized to result from a patient's unique immunological memory (Fierz & Walz, 2020; Kohler & Nara, 2020).

Reports of OAS in COVID-19 patient have largely focused on the phenomenon's beneficial or benign impacts on the immune response. For example, Abs from individuals naïve for SARS-CoV-2 infection, but exposed to other common human coronaviruses (hCoV), could cross-react with SARS-CoV-2 spike protein and neutralize SARS-CoV-2 pseudotypes (Ng et al., 2020). Plasma collected before the pandemic had Abs cross-reactive with SARS-CoV-2 nucleocapsid (NP) and spike proteins; these Abs did not confer protection against severe COVID-19 outcomes (Anderson et al., 2020). Though higher rates of prior cytomegalovirus and herpes simplex virus 1 infections have been reported for hospitalized COVID-19 patients versus patients with milder symptoms, no Ab signature linked to a molecular mechanism has been shown (Shrock et al., 2020). Humoral immunity to hCoVs, NL63 and 229E, has been associated with more severe COVID-19 disease (Focosi et al., 2021).

90 Recently, we reported the association of severe COVID-19 with the presence of Abs
91 binding specifically to a 21-mer peptide derived from SARS-CoV-2 NP, an epitope region termed
92 Ep9. The patients, described as αEp9(+), comprised about 27% of the sampled, SARS-CoV-2-
93 infected population (n = 186). The αEp9(+) patients (n = 34 in this report chosen for having
94 sufficient sample availability) had high, early levels of αN IgGs, typically within the first week,
95 compared to αEp9(-) patients; cytokine-related, immune hyperactivity also appeared in the
96 αEp9(+) individuals (Sen et al., 2021). These two observations suggest an OAS-based
97 mechanism for the disease severity observed in αEp9(+) patients. Here, we explore the epitope
98 homology landscape and αEp9 Ab cross-reactivity to potentially identify the original antigen
99 driving Ab-based immune response in αEp9(+) patients.

100 **Results and Discussion**

101 Assays measured levels of αEp9 IgGs and IgMs from αEp9(+) patients whose plasma was
102 collected at various times post-symptom onset (PSO). Consistent with the hallmarks of OAS
103 tracing a prior infection, αEp9 IgG levels appeared elevated as early as one day PSO in one
104 patient; similar IgG levels were observed in the patient population over >4 weeks (one-way
105 ANOVA, $p = 0.321$) (Figure 2A). Levels of αEp9 IgMs amongst patients at various times PSO
106 were also similar (one-way ANOVA, $p = 0.613$). The signals measured for αEp9 IgM levels were
107 significantly lower than the equivalent αEp9 IgG levels (t-test, $p = 0.0181$) (Figure 2B); this
108 difference could reflect lower IgM affinity, quantity, or both.

109 Searches for homologs to Ep9 in protein sequence and structural homology databases
110 suggested candidate primary antigens or potential OAS epitopes. The Basic Local Alignment
111 Sequence Tool (pBLAST) (Altschul et al., 1997) and Vector Alignment Search Tool (VAST)
112 (Madej et al., 2014) identified structurally homologous regions from betaherpesvirus 6A and 14
113 other proteins with Ep9 sequence homology spanning >7 residues. Additionally, Ep9-orthologous
114 regions from six common human coronaviruses (SARS-CoV, MERS, OC43, HKU-1, NL63, 229E)

115 were also chosen for production and assays (Figure 1 A, Figure 1- supplement 1). To expedite
116 the binding measurements, the potential OAS epitope regions were subcloned into phagemids
117 encoding the sequences as fusions to the M13 bacteriophage P8 coat protein. DNA sequencing
118 and ELISA experiments demonstrated successful cloning and consistent phage display,
119 respectively. Two of the 21 epitopes failed to display on phage and were omitted from subsequent
120 investigations (Figure 1- supplement 3A).

121 The potential OAS epitopes to αEp9 Abs were tested by phage ELISA. To assess average
122 response within a patient population, pooled plasma from three sets of five αEp9(+) and five
123 αEp9(-) COVID-19 patients were coated onto ELISA plates, and tested for binding to the phage-
124 displayed potential OAS epitopes. Commercially sourced plasma from healthy individuals
125 provided an additional negative control. Confirming previously reported results, SARS-COV-2
126 Ep9 along with a homologous epitope from SARS-CoV-1 (90% similarity) bound only to plasma
127 from αEp9(+) patients (Sen et al., 2021). Since only 75 cases of SARS-CoV-1 were reported in
128 the US during the 2003 outbreak, this binding is unlikely to drive OAS (World Health Organization,
129 2013).

130 The panel of potential epitopes revealed a candidate epitope from the neuraminidase (NA)
131 protein of an H3N2 influenza A strain, which circulated in 2014 (A/Para/128982-IEC/2014,
132 Accession No. AIX95025.1). This epitope is termed EpNeu here. The plasma from αEp9(-)
133 patients and healthy individuals did not bind to EpNeu ($p<0.0001$, two-way ANOVA *ad hoc* Tukey
134 test) (Figure 1C, D). Surprisingly, SARS-CoV-2 Ep9 and EpNeu share only 38% amino acid
135 sequence similarity. Other candidate epitope regions had significantly higher homology, but failed
136 to bind to αEp9(+) plasma (Figure 1- supplement 1).

137

138 **Figure 1**

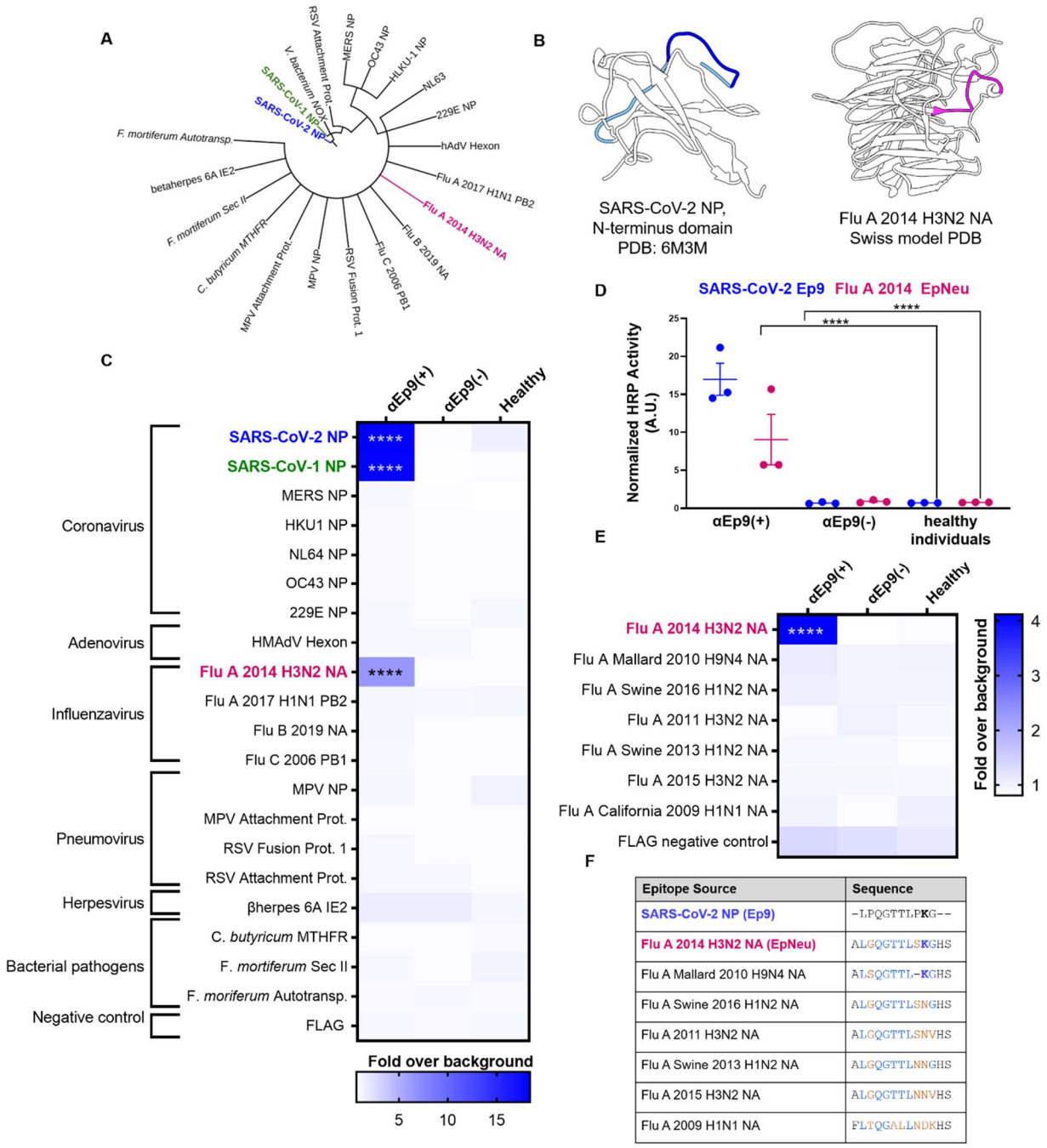

Epitope Source	Sequence
SARS-CoV-2 NP (Ep9)	-LPQGTTLPKG--
Flu A 2014 H3N2 NA (EpNeu)	ALGQGTTLSKGHS
Flu A Mallard 2010 H9N4 NA	ALSQGTTL-KGHS
Flu A Swine 2016 H1N2 NA	ALGQGTTLSNGHS
Flu A 2011 H3N2 NA	ALGQGTTLSNVHS
Flu A Swine 2013 H1N2 NA	ALGQGTTLNNGHS
Flu A 2015 H3N2 NA	ALGQGTTLNNVHS
Flu A 2009 H1N1 NA	FLTQGALLNDKHS

139

140 **Potential OAS epitopes for binding αEp9 Abs suggested by bioinformatics and tested by**
141 **phage ELISA.** (**A**) Cladogram depicting sequence homology of the Ep9 sequence from SARS-
142 CoV-2 to the bioinformatics-identified, closest homologs. Sequence alignments used pBLAST
143 and VAST, and the cladogram was generated by iTOL (Letunic & Bork, 2019). (**B**) Structures of
144 SARS-CoV-2 NP RNA binding domain (PDB: 6M3M) and the Flu A 2014 H3N2 NA protein
145 (modeled by SWISS-Model (Waterhouse et al., 2018)). SARS-CoV-2 NP highlights Ep9 residues

146 (light and dark blue) and the region homologous region to EpNeu (dark blue). The depicted model
147 of Flu A 2014 H3N2 NA highlights the EpNeu putative antigen (pink). (**C**) ELISAs examined
148 binding of phage-displayed potential OAS epitopes to Abs from three sets of pooled plasma from
149 five αEp9(+) patients, or five αEp9(-) patients. Pooled plasma from healthy patients was an
150 additional negative control. The colors of the heat map represent the mean binding signal
151 normalized to phage background negative controls (signal from phage without a displayed
152 peptide). (**D**) Expansion of data from panel C shows ELISA signals from the independently
153 assayed individual pools shows results from the individual pools (****p <0.0001 for a two-way
154 ANOVA comparing binding of phage-displayed epitopes listed in panel C to different groups of
155 pooled plasma, *ad hoc* Tukey test). (**E**) Using EpNeu as the search template to generate
156 homologous sequences (shown in next panel), ELISAs examined EpNeu homologs' binding to
157 pooled plasma from αEp9(+), αEp9(-), or healthy individuals. The data are represented as
158 described in panel C (****p <0.0001 for two-way ANOVA c phage-displayed epitopes, *ad hoc*
159 Tukey and Dunnett's test as shown). (**F**) Amino acid sequence alignment of the closely related
160 Flu A NA homologs of EpNeu from pBLAST(Altschul et al., 1997). Blue and orange residues
161 represent conserved and mismatched amino acids, respectively, relative to Ep9. Bolded residues
162 are important for epitope recognition by αEp9 Abs. Here, the term Flu refers to influenza.

163

164 The strain specificity of αEp9 Abs binding to H3N2 influenza A NA protein was tested next.
165 The EpNeu sequence provided the template for pBLAST homolog searching. Closely aligned NA
166 sequences isolated from human, avian, and swine hosts in North America were chosen for further
167 analysis (Figure 1F, Figure 1- supplement 1). The six sequences were phage-displayed as before.
168 Despite their close similarity to EpNeu (up to 92.3% similarity or only one residue difference),
169 none of the EpNeu homologs bound to Abs from αEp9(+) patients (Figure 1E). A single EpNeu
170 amino acid substitution, K142N (numbering from full-length NA, Accession No. AID57909.1)
171 occurs in an H1N2 swine flu from 2016; the single substitution dramatically decreased binding
172 affinity to Abs from αEp9(+) patients (p<0.0001 one-way ANOVA *ad hoc* Tukey). The epitope from
173 H4N6 avian influenza A from 2010 omits residue S141, but includes the conserved K142, also
174 greatly reduced binding to Abs from αEp9(+) patients (p<0.0001 one-way ANOVA *ad hoc* Tukey)
175 (Figure 1E, F). Therefore, S141 and K142 are critical for binding to αEp9 Abs.

176

177 **Figure 2**

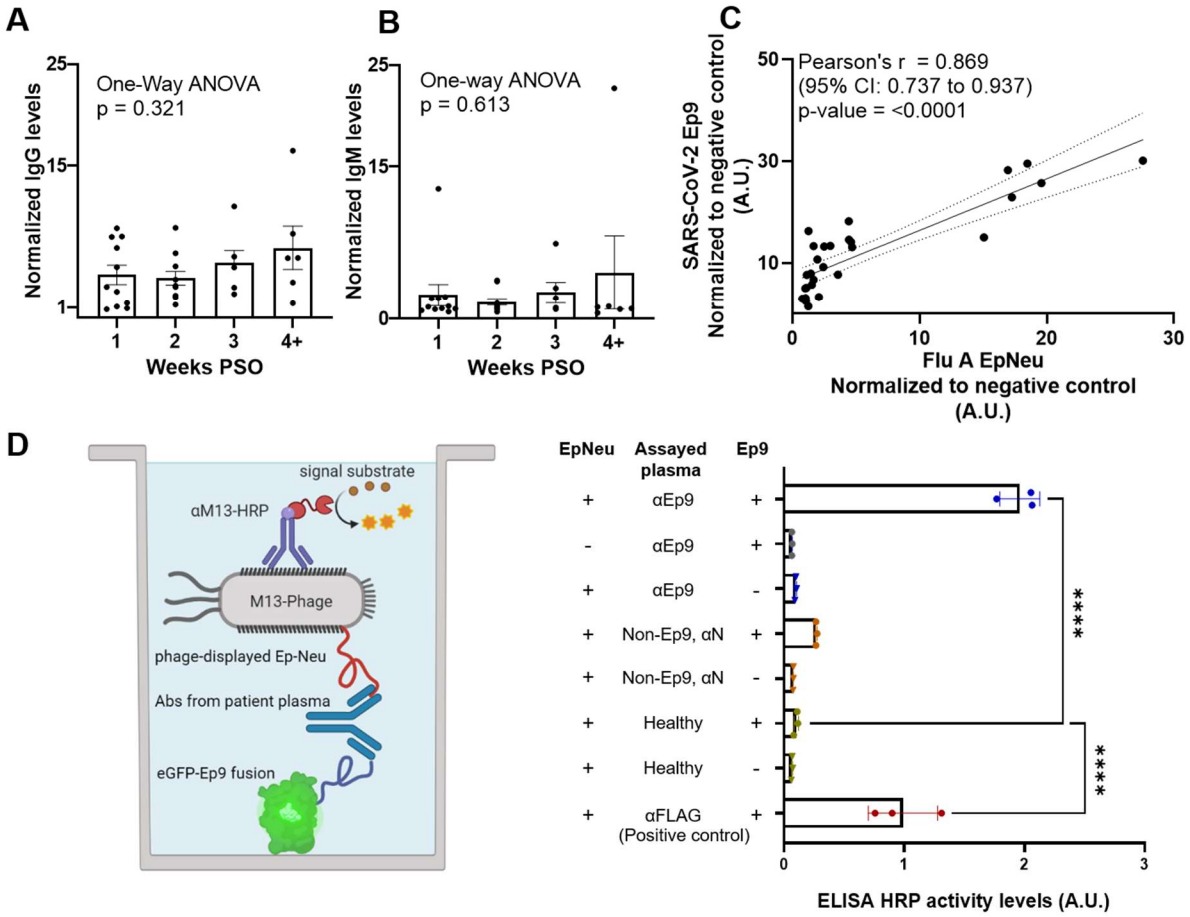

178
179 **Early upregulation of αEp9 IgGs and cross-reactive Ab binding to both Ep9 and EpNeu.**
180 ELISA of αEp9 (**A**) IgG and (**B**) IgM levels in αEp9(+) patients (n = 34) from plasma collected at
181 the indicated time periods post-symptom onset (PSO). Statistical analysis was conducted using
182 one-way ANOVA, *ad hoc* Tukey test. The solid line represents the median value, and dashed
183 lines represent quartiles. (**C**) Comparing normalized levels of phage-displayed Ep9 and EpNeu
184 binding to plasma-coated wells from individual αEp9(+) patients (n = 34). A strong correlation is
185 observed, as shown by the depicted statistics. Each point in panels A through C represents data
186 from individual patients. (**D**) A schematic diagram of the sandwich ELISA to examine cross-
187 reactivity of αEp9 Abs. The assay tests for bivalent Ab binding to both Ep9 and EpNeu. Pooled
188 plasma from five αEp9(+) patients or five αEp9(-) patients with other αNP Abs was tested for
189 bivalent binding to both eGFP-fused Ep9 and phage-displayed EpNeu. Healthy patient plasma
190 was used as a negative control. For additional negative controls, phage-FLAG and eGFP-FLAG
191 replaced Ep9 and EpNeu, respectively (****p <0.0001 one-way ANOVA, *ad hoc* Tukey and
192 Dunnett's test shown, with healthy plasma in the presence of EpNeu and Ep9 as negative control).
193 Error bars represent SD. Individual points on bar graph represent technical replicates.

194

195 Next, ELISAs were used to determine whether Ep9 and EpNeu epitopes bind to the same
196 Abs. Assays of 34 αEp9(+) patients demonstrated a strong and highly significant correlation

197 between levels of Abs binding to Ep9 and EpNeu epitopes in patient plasma, suggesting the two
198 epitopes may bind to the same Abs (Figure 2C). This cross-reactivity was confirmed by a
199 sandwich-format assay requiring bivalent, simultaneous binding by Abs to Ep9 and EpNeu (Figure
200 2D, Figure 2- supplement 1). In this assay, Ep9 was fused to the N-terminus of eGFP, and EpNeu
201 was phage-displayed. The results demonstrated binding of Abs to both Ep9 and EpNeu epitopes
202 in pooled plasma from αEp9(+) patients, but not in αEp9(-) patients with other αNP Abs or healthy
203 donors. Thus, we conclude that αEp9 Abs also recognize the EpNeu epitope region.

204 **Figure 3**
205

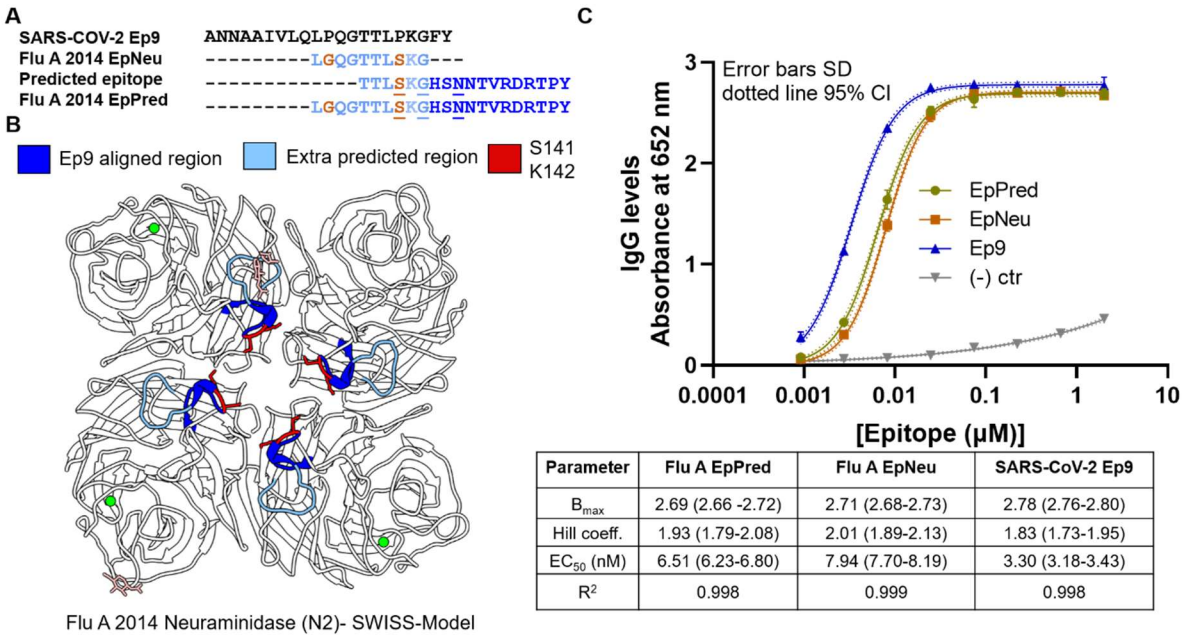

Parameter	Flu A EpPred	Flu A EpNeu	SARS-CoV-2 Ep9
B_{max}	2.69 (2.66 -2.72)	2.71 (2.68-2.73)	2.78 (2.76-2.80)
Hill coeff.	1.93 (1.79-2.08)	2.01 (1.89-2.13)	1.83 (1.73-1.95)
EC_{50} (nM)	6.51 (6.23-6.80)	7.94 (7.70-8.19)	3.30 (3.18-3.43)
R^2	0.998	0.999	0.998

206

207 **Binding interactions of αEp9 Abs with the predicted EpNeu epitope.** (**A**) Linear and structural
208 B-cell epitope prediction tools Bepipred 2.0 and Discotope 2.0 suggested an extended, linear
209 epitope region from the influenza A H3N2 2014 NA, including the eight residues of Ep9 Neu (light
210 blue) with an additional ten, C-terminal residues (dark blue). This extended, predicted epitope is
211 termed EpPred. Structural epitope predictions are underlined. Residues on EpNeu that are not
212 aligned with Ep9 are depicted in orange. (**B**) Structural model depicting the influenza A H3N2
213 2014 NA. The model was generated using SWISS-Model based on the NA structure from
214 influenza A H3N2 Tanzania 2010 (PDB: 4GZS). The NA structure highlights the EpNeu region
215 (light blue), the extended residues in EpPred (dark blue), potential glycosylation sites (light pink),
216 and the residues S141 and K142 (red), which are important for αEp9 Ab recognition. (**C**) Dose-
217 dependent ELISA comparing binding of αEp9 Abs to Ep9, EpNeu and EpPred. Pooled plasma
218 from five αEp9(+) patients and five αEp9(-) patients were tested in triplicates with varying
219 concentrations of eGFP-fused epitopes. The data demonstrates the strongest interactions

occurred between αEp9 Abs and Ep9 with an approximately 2-fold decrease in αEp9 Abs binding affinity for EpNeu. EpPred bound slightly stronger to αEp9 Abs than EpNeu; the difference in trend lines of EpNeu and EpPred are statistically significant ($p<0.0001$, Comparison of Fits). Trendlines represent non-linear regression fit with Hill slope analysis.

We then investigated whether EpNeu could present a viable antigen during the 2014 H3N2 (NCBI: txid1566483) infection. Linear epitope analysis of the whole NA protein using Bepipred 2.0 (Jespersen, Peters, Nielsen, & Marcatili, 2017) predicted a candidate antigen with eight residues from EpNeu, including S141 and K142 plus ten additional residues (146-155). This predicted epitope region, termed EpPred, includes the conserved catalytic NA residue D151 targeted for viral neutralization by the immune system (Gentles, Wan, Eichelberger, & Bloom, 2020) (Figures 3A, Figure 3- supplement 1A). Using a modelled structure of the 2014 H3N2 NA from Swiss-Model (Bienert et al., 2017; Guex, Peitsch, & Schwede, 2009; Studer et al., 2021; Waterhouse et al., 2018), the structural epitope prediction tool, Discotope 2.0 (Kringelum, Lundegaard, Lund, & Nielsen, 2012), also identified potential epitopes within EpPred (Figures 3A, Figure 3- supplement 1B).

EpPred was overexpressed as an eGFP-fusion protein (Figure 1-supplement 3B). Pooled plasma from five αEp9(+) patients was tested for Ab binding to EpPred, EpNeu, Ep9, and a negative control (eGFP FLAG). The αEp9 Abs bound to Ep9 with approximately two-fold higher apparent affinity than to EpNeu (Figure 3C). The increased binding strength of Ep9 could result from additional rounds of Ab affinity maturation post-primary infection (Brown & Essigmann, 2021). The longer length EpPred modestly improved upon the binding of EpNeu to αEp9 Abs (Figure 3C). Thus, αEp9 Abs likely target a larger epitope of H3N2 2014 NA beyond regions homologous to Ep9, though expression of NA makes this difficult to test (Lipničanová, Chmelová, Godány, Ondrejovič, & Miertuš, 2020). Furthermore, the phage-displayed and bacterially overexpressed epitopes applied here do not include post-translational modifications. Taken

246 together, the results support the hypothesis that the αEp9 Abs found in severe COVID-19 disease
247 may have originated from a primary infection with H3N2 influenza A.

248 Unfortunately, patient histories only rarely include previous influenza infections, and such
249 information was unavailable for patients in this study. The H3N2 2014 NA sequence was isolated
250 from Para, Brazil, and the strain's spread in North America remains unknown. However, a severe
251 outbreak of influenza A H3N2 was recorded; in 2014, an antigenic shift from the vaccine strain
252 A/Texas/50/2012(H3N2) resulted in low vaccine efficiency (14%), and high levels of other strains
253 spread (Flannery et al., 2016; Xie et al., 2015). Since only hemagglutinin was sequenced for strain
254 identification in 2014 (Flannery et al., 2016), the candidate OAS strain from the current
255 investigation could not be effectively traced as only its NA sequence was available. Our data
256 reveals that the EpNeu homologous sequence of the vaccine H3N2 strain (identical to Flu A 2015
257 H3N2 NA, Accession No. ANM97445.1) cannot bind αEp Abs (Figure 1 E, F). Therefore, αEp Abs
258 must have been generated against a primary influenza infection and not the vaccine.

259 This report offers a molecular mechanism for OAS underlying the high-rate of severe
260 COVID-19 in αEp9(+) patients. Specifically, we demonstrate cross-reactive binding between
261 αEp9 Abs and a predicted NA epitope from a 2014 influenza A strain. Interestingly, a study of an
262 Italian patient cohort correlated COVID-19 disease outcomes with previous RSV and
263 herpesviruses, but not influenza A infections (Wang et al., 2020). Future studies could examine
264 correlation between a country's rate of the H3N2 2014 influenza and severe COVID-19.
265 Additionally, health systems might have recorded such primary infections in specific patients,
266 which could also be searched for correlation. Examining epitope conservation and Ab cross-
267 reactivity could predict OAS-based immune responses and disease outcomes in future infections.
268 Identifying detrimental, benign or beneficial OAS pathways could also guide vaccine design for
269 increased efficacy and reduced risk.

270

271 ## Materials and Methods
272
273 ### Sequence and structural alignment analysis

274 To identify possible sources of primary infection responsible for αEp9 Ab generation,
275 sequence and structural alignment with Ep9 residues and the SARS-CoV-2 NP was conducted.
276 Alignment of Ep9 sequence with the orthologs from other human coronaviruses (hCoVs) such as
277 SARS-CoV, MERS, HKU-1, NL63, 229E and OC43 was conducted using the Benchling sequence
278 alignment tool (Benchling, 2017) (https://benchling.com). To explore a wider range of human host
279 pathogens pBLAST (Altschul et al., 1997) (https://blast.ncbi.nlm.nih.gov/Blast.cgi) was used to
280 search for Ep9 homology in a database of non-redundant protein sequences; common human-
281 host viruses were specified in the organism category. The queries were conducted with the blastp
282 (protein-protein BLAST) program (Altschul et al., 1997) with search parameters automatically
283 adjusted for short input sequences. Alignments spanning >7 residues were included here. The
284 Vector Alignment Search Tool (VAST) (Madej et al., 2014)
285 (https://structure.ncbi.nlm.nih.gov/Structure/VAST/vast.shtml) was used to find structural
286 alignment between SARS-CoV-2 Ep9 and proteins from other viral and bacterial human host
287 pathogens. Alignment for NP from common hCoV were not further examined, as they had been
288 included in sequence alignment analysis. The aligned sequences were sorted by the number of
289 aligned residues as well as root-mean square deviation (RMDS). The top 50 structurally aligned
290 proteins were then examined for structural homology in the Ep9 epitope region. Regions of
291 proteins that aligned with the Ep9 region were selected for subsequent analysis.
292

293 ### Cloning

294 Predicted OAS epitopes were subcloned for phage display using the pM1165a phagemid
295 vector (Levin, 2006) with an N-terminal FLAG-tag and a C-terminal P8 M13-bacteriophage coat
296 protein. OAS constructs were subcloned using the Q5 site-directed mutagenesis kit (New England
297 Biolabs, Ipswich, MA) as per manufacturer's instructions. After cloning, cells were transformed

298 into XL-1 Blue *E. coli* and spread on carbenicillin-supplemented (50 µg/ml) plates. Individual
299 colonies were then inoculated into 5 ml cultures, and shaken overnight at 37 °C. The phagemid
300 was isolated using the QIAprep spin miniprep kit (Qiagen, Germantown, MD) as per
301 manufacturer's instructions. Cloned sequences were verified by Sanger sequencing (Genewiz,
302 San Diego, CA).
303
304 **Phage propagation and purification**
305 The Ep9 homologs were expressed as N-terminal fusions to the P8 coat protein of M13
306 bacteriophage. Plasmids were transformed into SS320 *E. coli* and spread onto carbenicillin-
307 supplemented (50 µg/ml) LB-agar plates before overnight incubation at 37 °C. A single colony
308 was inoculated into a primary culture of 15 ml of 2YT supplemented with 50 µg/ml carbenicillin
309 and 2.5 µg/ml of tetracycline, and incubated at 37 °C with shaking at 225 rpm until an optical
310 density at 600 nm (OD_{600}) of 0.5 to 0.7 was reached. 30 µM IPTG and M13KO7 helper phage at
311 an MOI 4.6 was added to the primary culture, and the culture was incubated for an additional 37
312 °C with shaking at 225 rpm for 45 min. 8 ml of the primary culture was then transferred to 300 ml
313 of 2YT supplemented with 50 µg/ml of carbenicillin and 20 µg/ml of kanamycin. The cultures were
314 inoculated at 30 °C with shaking at 225 rpm for around 19 h.
315 The phage propagation culture was centrifuged at 9632 x *g* for 10 min at 4 °C. The
316 supernatant, containing the phage, was transferred into a separate tubes pre-aliquoted with 1/5th
317 volume of phage precipitation buffer (20% w/v PEG-8000 and 2.5 M NaCl), and incubated on ice
318 for 30 min. The solution, containing precipitated phage, was centrifuged for 15 min at 4 °C, and
319 the supernatant was discarded. The precipitated phage was centrifuged a second time at 1,541
320 x *g* for 4 min at 4 °C, and then dissolved in 20 ml of resuspension buffer (10 mM phosphate, 137
321 mM NaCl, pH 7.4 - 8.0 with Tween-20 0.05%, v/v and glycerol 10% v/v). The resuspended pellet
322 solution was divided into 1 ml aliquots, which were flash frozen with liquid nitrogen for storage in
323 -80 °C. Prior to use in ELISA binding assays, the aliquoted phage-displayed constructs were re-

324 precipitated in 0.2 ml of phage precipitation buffer after incubation for 30 min on ice. Aliquots were
325 centrifuged at 12298 x *g* for 20 min at 4 °C and the supernatant was discarded. The phage pellets
326 were re-centrifuged at 1968 x *g* for 4 min at 4 °C, and then resuspended in 1 ml of 10 mM
327 phosphate, 137 mM NaCl, pH 7.4.
328
329 **Expression and Purification of eGFP fusion peptides**
330 pET28c plasmids encoding eGFP fusions to C-terminal Ep9-FLAG, EpNeu-FLAG,
331 EpPred-FLAG and FLAG (negative control) and N-terminal His_6 peptide epitopes, were
332 transformed into BL21DE3 Star *E. coli* chemically competent cells. Transformants were spread
333 on carbenicillin-supplemented (50 μg/ml) LB-agar plates and incubated at 37 °C overnight. Single
334 colonies of each construct were selected to inoculate 25 ml LB media supplemented with
335 carbenicillin (50 μg/ml). After incubation at 37 °C with shaking at 255 rpm overnight, 5 ml of seed
336 cultures were used to inoculate 500 ml of LB media supplemented with carbenicillin (50 μg/ml).
337 Expression cultures were incubated at 37 °C with shaking at 225 rpm until an OD_{600} of ~0.5 was
338 reached. The cultures were induced with 0.5 mM IPTG and incubated at 25 °C for 18 h. The cells
339 were pelleted by centrifugation at 9632 x *g* for 20 min and resuspended in Tris-HCl lysis buffer
340 (20 mM Tris-HCl, 250 mM NaCl, pH 8). Cells were lysed by sonication and the insoluble fractions
341 were pelleted by centrifugation at 24696 x *g*. The supernatant was affinity-purified using
342 Profinity™ IMAC (BioRad, Hercules, CA) resin charged with nickel sulfate. The protein lysate was
343 batch bound overnight to the IMAC resin and purified using gravity columns. Columns were
344 washed with lysis buffer supplemented with 20 mM imidazole, and the elution fractions were
345 collected from lysis buffer containing 250 mM imidazole. The elution fractions were then buffer-
346 exchanged with lysis buffer lacking imidazole using Vivaspin® 20 Ultrafiltration Units (Sartorius,
347 Goettingen, Germany) with a molecular weight cutoff of 10 kDa. The final buffer imidazole

348 concentrations were calculated to be ~0.1 mM. Purified and buffer-exchanged protein fractions
349 were then visualized using 10% SDS-PAGE with Coomassie dye staining.
350
351 **Patient Sample Collection**

352 Samples were collected as previously described (Sen et al., 2021). Briefly, the UC Irvine
353 Experimental Tissue Resource (ETR) operates under a blanket IRB protocol (UCI #2012-8716)
354 which enables sample collection in excess of requirements for clinical diagnosis, and allows
355 distribution to investigators. Plasma was collected from daily blood draws of COVID(+) patients,
356 initially confirmed with pharyngeal swabs. After immediate centrifugation, plasma from heparin-
357 anticoagulated blood was stored for 3-4 days at 4 °C prior to its release for research use. Personal
358 health information was omitted and unique de-identifier codes were assigned to patients to comply
359 with the Non-Human Subjects Determination exemption from the UCI IRB. At the research facility,
360 SARS-CoV-2 virus in plasma samples was inactivated through treatment by incubation in a 56 °C
361 water bath for 30 min (Pastorino, Touret, Gilles, de Lamballerie, & Charrel, 2020) prior to storage
362 at -80 °C.
363
364 **Phage ELISAs**

365 As described in previous reports (Sen et al., 2021), pooled plasma from five αEp9(+) patients, five
366 αEp9(-) patients, or healthy patients (Sigma-Aldrich, Saint Louis, MO) were separately prepared
367 in coating buffer (50 mM Na_2CO_3, pH 9.6); the plasma was diluted 100-fold during this step.
368 Plasma samples were then immobilized in 96 well microtiter plates by shaking the plasma
369 solutions at 150 rpm at room temperature (RT) for 30 min. After aspiration and washing by plate
370 washer (BioTek, Winooski, VT), each well was blocked with 100 µL of ChonBlock Blocking Buffer
371 (CBB) (Chondrex, Inc., Woodinville, WA) for 30 mins, shaking at 150 rpm at RT. Wells were
372 subsequently washed three times with PBS-T (0.05% v/v Tween-20 in PBS). Next, 1 nM phage-

373 displayed candidate “original” epitopes and controls prepared in CBB was incubated in microtiter
374 wells for 1 h at RT with shaking at 150 rpm. Unbound phage were aspirated and removed using
375 three washes with PBS-T. The peroxidase-conjugated detection antibody, αM13-HRP (Creative
376 Diagnostics, Shirley, NY), was diluted 1000-fold in Chonblock Secondary Antibody Dilution
377 (Chondrex, Inc., Woodinville, WA) buffer; 100 µl of this solution was added to each well before
378 incubation for 30 min at RT with shaking at 150 rpm. Following aspiration and three washes (100
379 µl each), 1-Step Ultra TMB-ELISA Substrate Solution (ThermoScientific, Carlsbad, CA) was
380 added (100 µl per well). Absorbance of TMB substrate was measured twice at 652 nm by UV-Vis
381 plate reader (BioTek Winooski, VT) after 5 and 15 min of incubation. The experiment was
382 repeated three times using plasma from different αEp9(+) and αEp9(-) patients for each
383 experiments, using a total of 15 patients for each group. Each experiment was conducted in
384 technical duplicate.
385
386 **αEp9 IgG and IgM ELISA**
387 Plasma from 34 patients, previously tested for the presence of αEp9 Abs using phage
388 ELISAs (Sen et al., 2021), were used to test levels of αEp9 IgGs and IgMs. 2 µM eGFP-Ep9 or
389 eGFP-FLAG in PBS pH 8.0 were immobilized onto 96 well microtiter plates via overnight
390 incubation with shaking at 150 rpm at 4 °C. Excess protein was aspirated and removed with three
391 consecutive PBS-T washes. Wells were blocked by adding CBB (100 µl) before incubation at 30
392 min at RT with shaking at 150 rpm. Next, αEp9(+) patient plasma, diluted 1:100 in CBB (100 µl),
393 was added to duplicate wells before incubation at RT for 1 h with shaking at 150 rpm. The
394 solutions were discarded and sample wells were washed with PBS-T three times. αEp9 Abs
395 binding to the potential epitopes was detected using horse radish peroxidase (HRP) conjugated
396 αHuman Fc IgG (Thermo Fisher Scientific, Waltham MA) or αIgM µ-chain specific (Millipore
397 Sigma, Temecula, CA) Abs diluted 1:5000 in ChonBlock Sample Antibody Dilution buffer. 100 µl
398 of detection Abs were added to each sample well, and incubated for 30 min at RT with shaking at

399 150 rpm. Sample wells were aspirated and washed three times in PBS-T, and the binding signal
400 was detected after addition of TMB substrate (100 µl per well).
401
402 **Bivalent Abs binding ELISA**
403 eGFP-Ep9 or eGFP-FLAG was serially diluted (120 nM, 40 nM, 13 nM and 4 nM) in PBS
404 pH 8.0, and added to the appropriate wells in 96 well microtiter plates, followed by shaking
405 overnight at 150 rpm at 4 °C. Excess unbound protein was removed, and the plate was washed
406 three times in PBS-T. Wells were then blocked in CBB and incubated for 30 min at RT. After
407 blocking, pooled plasma (100 µl per well) from either five αEp9(+) patients, or five non-αEp9,
408 αNP(+) patients, or healthy individuals was added to the appropriate wells. Plasma from pooled
409 patients was diluted 100-fold in CBB. As a positive control αFLAG Ab was used as a 1:2000
410 dilution in CBB. Samples were incubated for 1 h at RT with 150 rpm shaking. The solution was
411 removed by aspiration, and the plate and washed three times with PBS-T. Then 1 nM EpNeu
412 displaying phage or the phage negative control with no epitopes displayed was diluted in CBB.
413 100 µl phage solution was added to microtiter wells and incubated for 30 min at RT with shaking
414 at 150 rpm. After aspirating and washing off unbound phage, binding of phage-displayed EpNeu
415 to plasma αEp9 Abs was visualized using αM13-HRP Ab diluted 1:10,000 in ChonBlock Sample
416 Antibody Dilution buffer. Samples were incubated for 30 min at RT with 150 rpm shaking, and
417 unbound Abs were removed through washing with PBS-T three times before addition of TMB
418 substrate (100 µl). Experiments were conducted in technical triplicates and repeated three times
419 with different αEp(+) and αEp(-) patient samples.
420
421 **Dose-dependent ELISA**
422 Wells of microtiter plates were coated with serially diluted concentration of eGFP-Ep9,
423 EpNeu and EpPred or eGFP-FLAG, and incubated overnight at 4 °C before blocking as described
424 above. Next, pooled plasma (100 µl per well) from either five αEp9(+) patients, or five αEp9(-)

425 patients, or healthy individuals at 1:100 total plasma dilution in CBB was added to the appropriate
426 wells. Samples were incubated for 1 h at RT with shaking at 150 rpm. After incubation, unbound
427 solution was removed, and the plates were washed three times with PBS-T. αEp9 IgG levels were
428 detected by adding αFc IgG-HRP diluted 1:5000 in ChonBlock Sample Dilution buffer, followed
429 by incubation for 30 min at RT with shaking at 150 rpm, followed by addition of TMB substrate
430 (100 µl per well). Experiments were conducted in technical triplicates and repeated three times
431 with different αEp(+) and αEp(-) patient samples.
432

433 **Linear B-cell Epitope Prediction**

434 Linear epitopes from the Influenza A/Para/128982-IEC/2014(H3N2) neuraminidase
435 protein were predicted using the partial sequence with Accession AIX95025.1 from the National
436 Center for Biotechnology Information's GenBank and the linear B-cell epitope prediction tool,
437 Bepipred 2.0 (Jespersen et al., 2017) (http://www.cbs.dtu.dk/services/BepiPred-2.0/). The
438 prediction thresholds were set to 0.5. The specificity and sensitivity of epitope prediction at this
439 threshold is 0.572 and 0.586, respectively.
440

441 **Structure-based B-cell epitope prediction**

442 The structure of Influenza A/Para/128982-IEC/2014(H3N2) neuraminidase protein was
443 modelled using Swiss-Model (Bertoni, Kiefer, Biasini, Bordoli, & Schwede, 2017; Bienert et al.,
444 2017; Guex et al., 2009; Studer et al., 2020, 2021; Waterhouse et al., 2018)
445 (https://swissmodel.expasy.org/interactive). Using the ProMod3 3.2.0 tool (Studer et al., 2021), a
446 structural model was generated based on the crystal structure (2.35Å, PDB 4GZS 1.A) of a
447 homologous H3N2 neuraminidase with 96.39% sequence identity. Modelling methods and quality
448 assessments are further detailed in the report below.
449 The structural model of Influenza A/Para/128982-IEC/2014(H3N2) neuraminidase was used to
450 predict structure-based epitopes. Using the *in silico* online platform Discotope 2.0 (Kringelum et

451 al., 2012) (http://www.cbs.dtu.dk/services/DiscoTope-2.0/), structure-based epitope propensity
452 scores were calculated to predict likely B-cell epitope residues. The score of -3.7 was set as the
453 threshold for epitope prediction, which estimates a specificity and sensitivity of 0.75 and 0.47,
454 respectively (Figure 3 – supplement 1).
455

456 **Statistical Analysis**

457 The ELISA data were analyzed in GraphPad Prism 9 (https://www.graphpad.com). Since
458 the ELISA assays of 21 potential OAS epitopes were conducted over several microtiter plates for
459 repeated experiments, the raw absorbance values for every patient sample were normalized and
460 represented as the ratio of phage negative control to the signal. For heatmaps, two-way Analysis
461 of variance (ANOVA) with a Tukey adjustment for multiple comparisons tests were conducted for
462 the entire dataset of epitopes. For column comparisons of two groups, for example IgM levels and
463 IgG levels in the αEp(+) patients, unpaired, two-tailed, parametric t-tests were applied.
464 Additionally, for column comparisons between more than two groups, for example IgM or IgG
465 levels groups by weeks PSO, One-way ANOVA with a Tukey adjustment for multiple comparisons
466 tests were used. Where indicated, an ANOVA with a Dunnett's adjustment were performed to
467 compare results to healthy Abs interactions to αEp9(+) patient results. Graphs represent SD error
468 bars for technical replicates, defined as replicates of the same conditions in multiple wells of the
469 same plate. Whereas error bars are shown as SEM when an experiment is repeated with different
470 patient sample sets. Correlations between Ep9 and EpNeu levels in patients were determined by
471 plotting normalized values on an XY graph and performing a linear Pearson's correlation
472 coefficient test, where a *r* coefficient between 1.0-0.7 were considered strong correlations, values
473 between 0.7 and 0.5 were considered a moderate correlation, and values below 0.5 were
474 considered a weak correlation (Mukaka, 2012). The significance of the correlation was evaluated
475 based on p-value <0.05.

476 **Figure 1-supplement 1: Potential "original" epitopes targeted by αEp9 Abs**

Construct #	Pathogen	Target protein	Accession No.	Residues	Epitope sequences	Similarity %
Phage-displayed constructs						**template: Ep9 or EpNeu**
1	SARS-COV-2 (Ep9)	Nucleocapsid	QQX29443.1	152-172	ANNAAIVLQLPQGTTLPKGFY	-
2	SARS-COV-1	Nucleocapsid	YP_009825061.1	153-173	NNNAATVLQLPQGTTLPKGFY	90.5
3	MERS	Nucleocapsid	YP_009047211.1	141-151	NNDSAIVTQFAPGTKLPKNFH	66.7
4	Human coronavirus HKU1	Nucleocapsid	YP_173242.1	166-186	TTQEAIPTRFPPGTILPQGYY	57.1
5	Human coronavirus NL63	Nucleocapsid	YP_003771.1	119-136	NQKPLEPKFSIALPPELS	13.8
6	Human coronavirus OC43	Nucleocapsid	YP_009555245.1	167-187	SSDEAIPTRFPPGTVLPQGYY	71.4
7	Human coronavirus 229E	Nucleocapsid	AGW80953.1	122-138	SEPEIPHFNQKLPNGVT	21.4
8	Human adenovirus 61	Hexon	AQQ81927.1	123-164	ANNAATPQVVFYTEDVNLEMPDTHLVFKPAVPNGTIASESLL	17.6
9	Human mastadenovirus E	PVIII	YP_068038.1	76-114	AALVYQEIPQPTTVLLPRDAQAEVQLTNSGVQLAGGATL	31
10	Influenza A virus (A/Utah/40/2017)	PB2 polymerase	AVH77902.1	225-244	GSVYIEVLHLTQGTCWEQMY	41.7
11	Influenza A virus (EpNeu) (A/Para/128982-IEC/2014(H3N2)	Neuraminidase, partial	AIX95025.1	34-46	ALGQGTTLSKGHS	38.1
12	Influenza B virus (B/California/88/2019)	Neuraminidase	QIA55965.1	67-79	ATKGVVLLLPEPE	28.6
13	Influenza C virus (C/Singapore/DSO-070193/2006)	Polymerase PB1, partial	AFV68302.1	119-145	AATALQLTVDAIKETEGPFKGTTMLEY	34.4
14	Human respiratory syncytial virus A	Fusion protein	ASU44644.1	87-100	NNAVTELQLLMQST	38.1
15	Human respiratory syncytial virus A	Attachment glycoprotein	ART28426.1	106-116	GTTPQSTTIPA	28.6
16	Human metapneumovirus	Nucleoprotein, partial	ABO15448.1	11-33	TTTAVTPSSLPQEITLLCGEILY	34.8
17	Human metapneumovirus	Attachment glycoprotein, partial	AEW90340.1	57-72	PQQTTDKHTALPKSIY	30.8
18	Human betaherpesvirus 6A	Immediate Early protein 2	AGJ52064.1	1396-1422	AATPIDFVGAVKTCNKYAKDNPKEIVL	10
19	Verrucomicrobia bacterium	NADH-quinone oxidoreductase (NOX)	PYJ45937.1	76-89	AGVVLQLPQGTTL	57.1

477

478

20	Clostridium butyricum	Bifunctional methylenetetrahydrofolate dehydrogenase/methenyltetrahydrofolate cyclohydrolase (MTHFD2)	MBE6063617.1	94-104	IILQLPLPKKF	**47.6**
21	Fusobacterium mortiferum	Type II secretion protein	WP_118233983.1	77-99	VENGAIVLQYDKEIYLGLTENFF	**48**
22	Fusobacterium mortiferum	Autotransporter outer membrane protein	WP_005886362.1	449-460	NGAIVGDLVQGT	**38.1**
23	Influenza A virus (A/swine/Missouri/A01774733/2016(H1N2) or A/Para/129501-IEC/2014(H3N2))	Neuraminidase	ANK78229.1 / AIX95013	133-145/ 24-36	ALGQGTTLSNGHS	**92.3**
24	Influenza A (A/swine/Minnesota/A01394278/2013(H3N2))	Neuraminidase	AHA57095.1	134-146	ALGQGTTLNNGHS	**92.3**
25	Influenza A virus (A/California/04/2009 (H1N1))	Neuraminidase	AJI76397.1	75-89	TFFLTQGALLNDKHS	**46.7**
26	Influenza A virus (A/California/111/2015(H3N2))	Neuraminidase	ANM97445.1	133-145	ALGQGTTLNNVHS	**84.6**
27	Influenza A virus (A/mallard/California/1156/2010(H4N6))	Neuraminidase	AEK50939.1	133-142	ALSQGTTLKG	**84.6**
28	Influenza A virus (A/California/33/2011(H3N2))	Neuramidase	AGL06761.1	133-145	ALGQGTTLSNVHS	**84.6**
29	Influenza A virus (**EpNeu Pred**) (A/Para/128982-IEC/2014(H3N2))	Neuraminidase, partial	AIX95025.1	34-56	ALGQGTTLSKGHSNNTVRDRTPY	**-**
eGFP-fusion constructs						
30	Influenza A virus (**EpNeu**) (A/Para/128982-IEC/2014(H3N2))	Neuraminidase	AIX95025.1	34-46	ALGQGTTLSKGHS	**-**
31	Influenza A virus (**EpNeu Pred**) (A/Para/128982-IEC/2014(H3N2))	Neuraminidase	AIX95025.1	34-56	ALGQGTTLSKGHSNNTVRDRTPY	**-**

479

480 **Figure 1 –supplement 2: Primers used to subclone potential original epitopes**

Construct #	Primer names:	Oligonucleotide sequence
Phage-displayed constructs		
1	primer_1_F	tcaagggactaccttgcccaaggggttctatGGTGGAGGATCCGGGAGC
	primer_1_R	ggtaattgtaacacgattgcagcgttattagcTCCACTTCCTTTATCATCGTCATCTTTATAATC
2	primer_2_F	acttccacagggaacgacactgccaaagggatttGGTGGAGGATCCGGGAGC
	primer_2_R	tgcagtacagtggcagcattgttatttccacttccTTTATCATCGTCATCTTTATAATCAACCAATGC
3	primer_3_F	tccgggtacaaagttaccaaagaacttccacGGTGGAGGATCCGGGAGC
	primer_3_R	gcaaattgagtaactatcgctgaatcattgttTCCACTTCCTTTATCATCGTCATCTTTATAATC
4	primer_4_F	tcccggaactattttaccccaaggatactatGGTGGAGGATCCGGGAGC
	primer_4_R	gggaatctagtgggaatcgcctcctgagtagtTCCACTTCCTTTATCATCGTCATCTTTATAATC
5	primer_5_F	agtattgccttgccacctgagttatctGGTGGAGGATCCGGGAGC
	primer_5_R	aaatttcggttcaagcggcttttgattTCCACTTCCTTTATCATCGTCATCTTTATAATC
6	primer_6_F	tccgggtactgttttgcctcagggttactacGGTGGAGGATCCGGGAGC
	primer_6_R	ggaaaccgcgttgggatggcctcatcagagctTTTATCATCGTCATCTTTATAATCAACCAATGC
7	primer_7_F	ccagaaattgccgaacggcgttactGGTGGAGGATCCGGGAGC
	primer_7_R	ttaaagtgagggatctctggctcgctTTTATCATCGTCATCTTTATAATCAACCAATGC
8	primer_8_F	TTCTAAATTCACATCCTCAGTATAGAACACGACTTGTGGGGTTGCTGCATTGTTGGCTTTATCATCGTCATCTTTATAATCAACCAATGC
	primer_8_R	ATGCCAGATACTCATTTGGTCTTCAAACCTGCGGTCCCGAATGGCACGATTGCTAGTGAATCTCTCCTCggtggaggatccgggagc
9	primer_9_F	ACGCGGGAGCAGCACTGTAGTCGGCTGAGGGATTTCCTGGTACACCAGGGCGGCTTTATCATCGTCATCTTTATAATCAACCAATGC
	primer_9_R	GACGCGCAAGCCGAGGTCCAGTTGACAAACAGCGGTGTACAATTGGCTGGCGGTGCCACTCTGggtggaggatccgggagc
10	primer_10_F	acacaaggcacttgctgggagcaaatgtatGGTGGAGGATCCGGGAGC
	primer_10_R	gaggtgcagcacttcaatatagactgacccTTTATCATCGTCATCTTTATAATCAACCAATGC
11	primer_11_F	gctttctaagggccacagcGGTGGAGGATCCGGGAGC
	primer_11_R	gtggtgccttggcccaatgcTTTATCATCGTCATCTTTATAATCAACCAATGC
12	primer_12_F	gctgcttccggagccagagGGTGGAGGATCCGGGAGC
	primer_12_R	agcacgacgcctttcgtagcTTTATCATCGTCATCTTTATAATCAACCAATGC
13	primer_13_F	gactgaaggtccttttaagggcacgacaatgttggaatatGGTGGAGGATCCGGGAGC
	primer_13_R	tctttaatggcatcgaccgtaagttggagagccgtcgctgcTTTATCATCGTCATCTTTATAATCAACCAATGC
14	primer_14_F	caactcctcatgcagtctacaGGTGGAGGATCCGGGAGC
	primer_14_R	aagttctgtgacagcattgttTTTATCATCGTCATCTTTATAATCAACCAATGC
15	primer_15_F	gacaaccatccctgcaGGTGGAGGATCCGGGAGC
	primer_15_R	gattgaggcgtagtcccTTTATCATCGTCATCTTTATAATCAACCAATGC
16	primer_16_F	ggaaatcactctcttgtgcggcgaaatcttatatGGTGGAGGATCCGGGAGC
	primer_16_R	tgcggcaggctagatggcgtaactgccgtagtagtTTTATCATCGTCATCTTTATAATCAACCAATGC
17	primer_17_F	acggcactgccgaagtccatctacGGTGGAGGATCCGGGAGC
	primer_17_R	atgcttgtcagtggtctgttgtggTTTATCATCGTCATCTTTATAATCAACCAATGC
18	primer_18_F	caacaaatacgctaaggacaatccgaaagagatcgtgcttGGTGGAGGATCCGGGAGC
	primer_18_R	caggtcttgacagctccgacgaagtcgatgggcgtagccgcTTTATCATCGTCATCTTTATAATCAACCAATGC
19	primer_19_F	tccacaaggcaccacccttGGTGGAGGATCCGGGAGC
	primer_19_R	agctgcagcacgacgccggcTTTATCATCGTCATCTTTATAATCAACCAATGC
20	primer_20_F	gttacctaagaaattcGGTGGAGGATCCGGGAGC
	primer_20_R	ggaagctgcaaaataatTTTATCATCGTCATCTTTATAATCAACCAATGC
21	primer_21_F	agagatttacctggggctgacagagaactttttGGTGGAGGATCCGGGAGC
	primer_21_R	ttgtcgtactgtaatacaattgcgccgttctccacTTTATCATCGTCATCTTTATAATCAACCAATGC
22	primer_22_F	gatttagtacagggtaccGGTGGAGGATCCGGGAGC
	primer_22_R	gcctacaatggcaccattTTTATCATCGTCATCTTTATAATCAACCAATGC
23	primer_23_F	CGCTTTCTAAtGGCCACAGCG
	primer_23_R	TGGTGCCTTGGCCCAATG
24	primer_24_F	CACCACGCTTaacaatGGCCACAGCG
	primer_24_R	CCTTGGCCCAATGCTTTAT
25	primer_25_F	tcttttgaacgacaagcattcaGGTGGAGGATCCGGGAGC
	primer_25_R	gctccctgagtcagaaagaatgtTTTATCATCGTCATCTTTATAATCAACCAATGC
26	primer_26_F	attaaataacgttcatagtGGTGGAGGATCCGGGAGC
	primer_26_R	gtagtaccctggcccaaggcTTTATCATCGTCATCTTTATAATCAACCAATGC
27	primer_27_F	tgcgaacggtacgattcatgatcgttccccattcGGTGGAGGATCCGGGAGC
	primer_27_R	tgacgacctttcagtgtcgtgccttgagataacgcTTTATCATCGTCATCTTTATAATCAACCAATGC
28	primer_28_F	tttgtcgaatgtacactccGGTGGAGGATCCGGGAGC
	primer_28_R	gtggtaccctggccaagagcTTTATCATCGTCATCTTTATAATCAACCAATGC
29	primer_29_F	ctcgaacaacaccgttcgcgaccgtactccgtacGGTGGAGGATCCGGGAGC
	primer_29_R	tgccctttagacagagttgtcccttggcccaaagcTTTATCATCGTCATCTTTATAATCAACCAATGC
eGFP-fusion constructs		
30	primer_30_F	gctttctaagggccacagcAGCGGAAGTGGAGATTATAAAGATGAC
	primer_30_R	gtggtgccttggcccaatgcGGAGCTCCCGGATCCTCC
31	primer_31_F	ctcgaacaataccgtccgcgatcggactccgtacAGCGGAAGTGGAGATTATAAAGATGAC
	primer_31_R	tgaccttgctcaaagtagtaccctgcccaagcgcGGAGCTCCCGGATCCTCC

481 **Figure 1 – supplement 3**

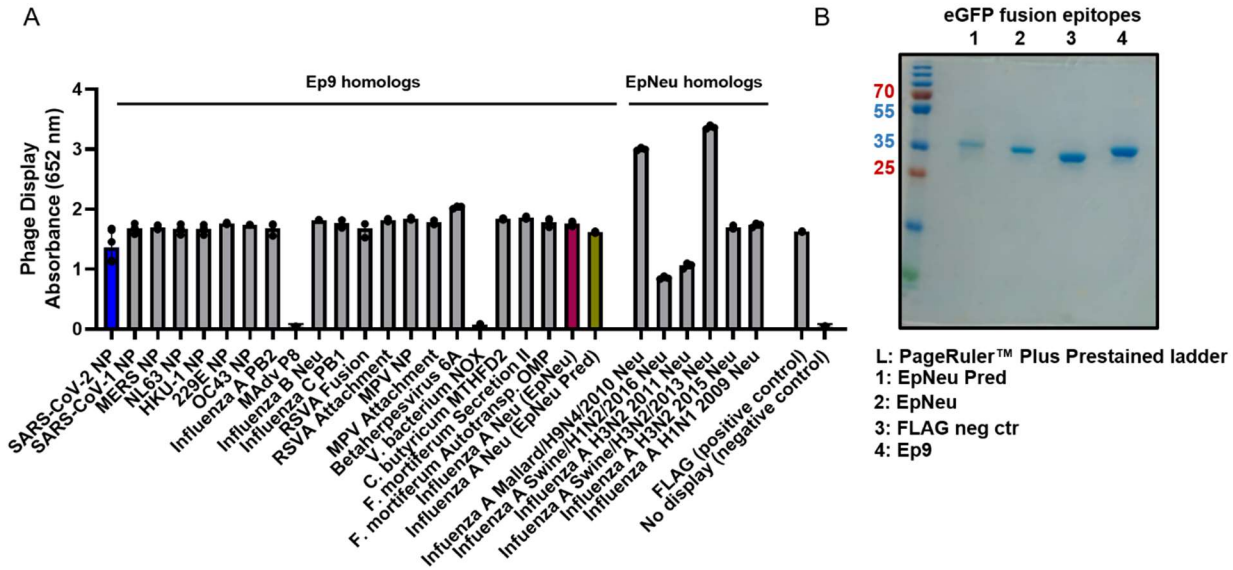

482

483 **Expression of phage-displayed and eGFP-fused potential OAS epitopes.** (**A**) ELISA
484 demonstrating the display of N-terminal FLAG-tagged potential epitopes fused to the N-
485 terminus of the P8 coat protein. Immobilized αFLAG Abs in microtiter wells bind the
486 displayed FLAG-tag and epitope, and binding is detected with αM-13-HRP Abs as usual.
487 Phage with no epitope displayed provide the negative control. Epitopes for
488 mastadenovirus protein (mAdV) P8 and *V. bacterium* NADH oxidoreductase (NOX) did
489 not display. Error bars represent SD values. (**B**) 10% SDS-PAGE gel stained with
490 Coomassie Blue shows His-tag affinity-purified and buffer-exchanged eGFP-fused
491 epitopes, EpPred, EpNeu, FLAG negative control and Ep9.

492

493

494

495

496

497

498 **Figure 2 –supplement 1**

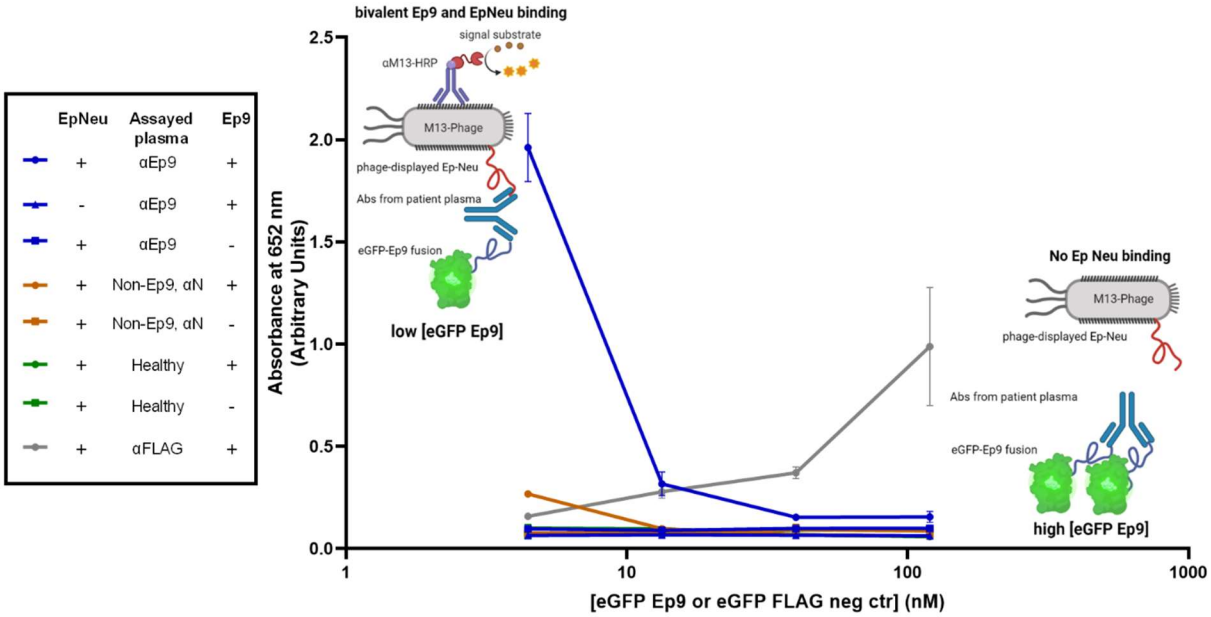

499

500 **Optimization of assay to determine cross-reactivity of αEp9 Ab to Ep9 and EpNeu.**
501 Sandwich ELISA testing the binding of Abs from the pooled plasma of five αEp9(+)
502 patients, five αEp9(-) patients with other αNP Abs and healthy individuals. This
503 experiment examines bivalent binding to various doses of immobilized eGFP-fused Ep9
504 epitope (120, 40, 13 and 4 nM) and phage-displayed EpNeu in solution. The data shows
505 that Abs from αEp9(+) patients, but not αEp9(-) or healthy individuals, bivalently bind
506 both EpNeu and Ep9. The positive control (αFLAG 1:2000 fold dilution) at 100 nM eGFP
507 demonstrates concentrations appropriate for bivalent binding to immobilized and in-
508 solution tags. The schematic diagram illustrates the binding observed for bivalence in
509 αEp9 Abs, where the antibody bridges plate-bound eGFP at its high concentrations.
510 Therefore, Figure 2 in the main text uses 4 nM of eGFP Ep9 coated on the plate, and the
511 FLAG positive control uses eGFP at 100 nM. Error bars represent SD.

512

513

514

515

516

517 **Figure 3 –supplement 1**

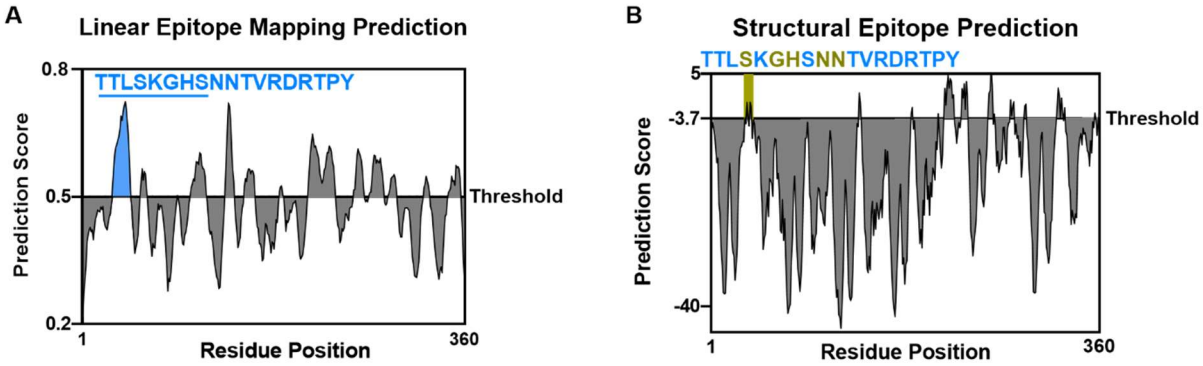

518

519 **Linear and structural epitope mapping prediction of Influenza A H3N2**
520 **Neuraminidase.** (**A**) Linear epitope mapping prediction of the Flu A 2014 H3N2 using
521 Bepipred 2.0 (Jespersen et al., 2017) demonstrates high prediction scores in a region
522 spanning 18 residues, which includes eight residues from EpNeu (underlined). The
523 additional 10 predicted residues were included as part of an extended epitope termed
524 EpPred. (**B**) Structural epitope mapping, using Discotope 2.0 (Kringelum et al., 2012), of
525 the modelled neuraminidase protein from Flu A 2014 H3N2 (SWISS-model
526 (Waterhouse et al., 2018)), predicts an epitope of five residues. These were captured by
527 EpPred, including three found in EpNeu.
528

References

Altschul, S. F., Madden, T. L., Schäffer, A. A., Zhang, J., Zhang, Z., Miller, W., & Lipman, D. J. (1997). Gapped BLAST and PSI-BLAST: A new generation of protein database search programs. *Nucleic Acids Research*. https://doi.org/10.1093/nar/25.17.3389

Anderson, E. M., Goodwin, E. C., Verma, A., Arevalo, C. P., Bolton, M. J., Weirick, M. E., … Vanderbeck, A. N. (2020, November). Seasonal human coronavirus antibodies are boosted upon SARS-CoV-2 infection but not associated with protection. *MedRxiv*. medRxiv. https://doi.org/10.1101/2020.11.06.20227215

Benchling, I. (2017). Benchling [Biology Software].

Bertoni, M., Kiefer, F., Biasini, M., Bordoli, L., & Schwede, T. (2017). Modeling protein quaternary structure of homo- and hetero-oligomers beyond binary interactions by homology. *Scientific Reports*. https://doi.org/10.1038/s41598-017-09654-8

Bienert, S., Waterhouse, A., De Beer, T. A. P., Tauriello, G., Studer, G., Bordoli, L., & Schwede, T. (2017). The SWISS-MODEL Repository-new features and functionality. *Nucleic Acids Research*. https://doi.org/10.1093/nar/gkw1132

Brown, E. L., & Essigmann, H. T. (2021). Original Antigenic Sin: the Downside of Immunological Memory and Implications for COVID-19. *MSphere*, *6*(2). https://doi.org/10.1128/mSphere.00056-21

Fierz, W., & Walz, B. (2020). Antibody Dependent Enhancement Due to Original Antigenic Sin and the Development of SARS. *Frontiers in Immunology*, *11*, 1120. https://doi.org/10.3389/fimmu.2020.01120

Flannery, B., Zimmerman, R. K., Gubareva, L. V., Garten, R. J., Chung, J. R., Nowalk, M. P., … Fry, A. M. (2016). Enhanced Genetic Characterization of Influenza A(H3N2) Viruses and Vaccine Effectiveness by Genetic Group, 2014-2015. In *Journal of Infectious Diseases* (Vol. 214, pp. 1010–1019). Oxford University Press. https://doi.org/10.1093/infdis/jiw181

Focosi, D., Genoni, A., Lucenteforte, E., Tillati, S., Tamborini, A., Spezia, P. G., … Maggi, F. (2021). Previous Humoral Immunity to the Endemic Seasonal Alphacoronaviruses NL63 and 229E Is Associated with Worse Clinical Outcome in COVID-19 and Suggests Original Antigenic Sin. *Life*. https://doi.org/10.3390/life11040298

Gentles, L. E., Wan, H., Eichelberger, M. C., & Bloom, J. D. (2020, May 9). Antibody neutralization of an influenza virus that uses neuraminidase for receptor binding. *BioRxiv*. bioRxiv. https://doi.org/10.1101/2020.05.08.084954

Guex, N., Peitsch, M. C., & Schwede, T. (2009). Automated comparative protein structure modeling with SWISS-MODEL and Swiss-PdbViewer: A historical perspective. *Electrophoresis*. https://doi.org/10.1002/elps.200900140

Jespersen, M. C., Peters, B., Nielsen, M., & Marcatili, P. (2017). BepiPred-2.0: Improving sequence-based B-cell epitope prediction using conformational epitopes. *Nucleic Acids Research*. https://doi.org/10.1093/nar/gkx346

Kohler, H., & Nara, P. (2020, August 1). A Novel Hypothesis for Original Antigenic Sin in the Severe Disease of SARS-CoV-2 Infection. *Monoclonal Antibodies in Immunodiagnosis and Immunotherapy*. Mary Ann Liebert Inc. https://doi.org/10.1089/mab.2020.0029

Kringelum, J. V., Lundegaard, C., Lund, O., & Nielsen, M. (2012). Reliable B Cell Epitope Predictions: Impacts of Method Development and Improved Benchmarking. *PLoS*

Computational Biology, *8*(12). https://doi.org/10.1371/journal.pcbi.1002829

Letunic, I., & Bork, P. (2019). Interactive Tree of Life (iTOL) v4: Recent updates and new developments. *Nucleic Acids Research*, *47*(W1), W256–W259. https://doi.org/10.1093/nar/gkz239

Levin, A. M. (2006). Exploring the interaction between the protein kinase A catalytic subunit and caveolin-1 scaffolding domain with shotgun scanning, oligomer complementation, NMR, and docking. *Protein Science*. https://doi.org/10.1110/ps.051911706

Lipničanová, S., Chmelová, D., Godány, A., Ondrejovič, M., & Miertuš, S. (2020). Purification of viral neuraminidase from inclusion bodies produced by recombinant Escherichia coli. *Journal of Biotechnology*, *316*, 27–34. https://doi.org/10.1016/j.jbiotec.2020.04.005

Madej, T., Lanczycki, C. J., Zhang, D., Thiessen, P. A., Geer, R. C., Marchler-Bauer, A., & Bryant, S. H. (2014). MMDB and VAST+: Tracking structural similarities between macromolecular complexes. *Nucleic Acids Research*, *42*(D1). https://doi.org/10.1093/nar/gkt1208

Mukaka, M. M. (2012). Statistics corner: A guide to appropriate use of correlation coefficient in medical research. *Malawi Medical Journal*.

Ng, K. W., Faulkner, N., Cornish, G. H., Rosa, A., Harvey, R., Hussain, S., … Kassiotis, G. (2020). Preexisting and de novo humoral immunity to SARS-CoV-2 in humans. *Science*, *370*(6522), 1339–1343. https://doi.org/10.1126/science.abe1107

Park, M. S., Kim, J. Il, Park, S., Lee, I., & Park, M. S. (2016). Original antigenic sin response to RNA viruses and antiviral immunity. *Immune Network*. Korean Association of Immunologists. https://doi.org/10.4110/in.2016.16.5.261

Pastorino, B., Touret, F., Gilles, M., de Lamballerie, X., & Charrel, R. N. (2020). Heat inactivation of different types of SARS-CoV-2 samples: What protocols for biosafety, molecular detection and serological diagnostics? *Viruses*, *12*(7), 735–743. https://doi.org/10.3390/v12070735

Sen, S. R., Sanders, E. C., Gabriel, K. N., Miller, B. M., Isoda, H. M., Salcedo, G. S., … Weiss, G. A. (2021). Predicting COVID-19 Severity with a Specific Nucleocapsid Antibody plus Disease Risk Factor Score. *MSphere*, *6*(2), e00203-21. https://doi.org/10.1128/mSphere.00203-21

Shrock, E., Fujimura, E., Kula, T., Timms, R. T., Lee, I.-H., Leng, Y., … Elledge, S. J. (2020). Viral epitope profiling of COVID-19 patients reveals cross-reactivity and correlates of severity. *Science*, eabd4250. https://doi.org/10.1126/science.abd4250

Studer, G., Rempfer, C., Waterhouse, A. M., Gumienny, R., Haas, J., & Schwede, T. (2020). QMEANDisCo—distance constraints applied on model quality estimation. *Bioinformatics*. https://doi.org/10.1093/bioinformatics/btz828

Studer, G., Tauriello, G., Bienert, S., Biasini, M., Johner, N., & Schwede, T. (2021). ProMod3 - A versatile homology modelling toolbox. *PLoS Computational Biology*. https://doi.org/10.1371/JOURNAL.PCBI.1008667

Wang, L., Candia, J., Ma, L., Zhao, Y., Imberti, L., Sottini, A., … Zhang, Y. (2020). Serological responses to human virome define clinical outcomes of italian patients infected with SARS-CoV-2. *MedRxiv*. https://doi.org/10.1101/2020.09.04.20187088

Waterhouse, A., Bertoni, M., Bienert, S., Studer, G., Tauriello, G., Gumienny, R., … Schwede, T. (2018). SWISS-MODEL: Homology modelling of protein structures and

621 complexes. *Nucleic Acids Research*. https://doi.org/10.1093/nar/gky427
622 Welsh, R. M., & Fujinami, R. S. (2007). Pathogenic epitopes, heterologous immunity and
623 vaccine design. *Nature Reviews Microbiology*, *5*(7), 555–563.
624 https://doi.org/10.1038/nrmicro1709
625 World Health Organization. (2013). WHO | Cumulative Number of Reported Probable
626 Cases of Severe Acute Respiratory Syndrome (SARS). Retrieved May 16, 2021,
627 from http://www.who.int/csr/sars/country/en/
628 Xie, H., Wan, X. F., Ye, Z., Plant, E. P., Zhao, Y., Xu, Y., … Zhu, Y. (2015). H3N2
629 Mismatch of 2014-15 Northern Hemisphere Influenza Vaccines and Head-to-head
630 Comparison between Human and Ferret Antisera derived Antigenic Maps. *Scientific*
631 *Reports*, *5*(1), 1–10. https://doi.org/10.1038/srep15279
632